Check for updates

Efficient photoelectrocatalytic performance of beta-cyclodextrin/graphene composite and effect of Cl⁻ in water: degradation for bromophenol blue as a case study†

Qiao Cong,[a] Miao Ren,[b] Tingting Zhang,[b] Fangyuan Cheng[b] and Jiao Qu [iD] *[b]

Photoelectrocatalytic technology has proven to be an efficient way of degrading organic contaminants, including dyes. Graphene (GR) -based catalysts have been frequently used in photoelectrocatalysis, due to their excellent catalytic performances. In this work, the GR/beta-cyclodextrin (GR/β-CD) composite was prepared and used for a widely used triphenylmethane dye (bromophenol blue, BPB) photoelectrocatalytic degradation. The results indicated that the degradation of the prepared GR/β-CD composite for BPB was effective with the combination of external bias voltage and simulated sunlight irradiation. Under optimum conditions, the BPB (10 mg L^{-1}) was completely eliminated by GR/β-CD composite within 120 min. $^{\bullet}O_2^{-}$ played a prominent role in the BPB photoelectrocatalytic degradation. The time required for the removal of BPB in water to reach 100% can be reduced to 30 min with the presence of Cl^{-}, owing to the generation of $^{\bullet}$Cl. Moreover, the toxicity of the degraded system with Cl^{-}, predicted by the QSAR (Quantitative Structure–Activity Relationship) model in ECOSAR (Ecological Structure–Activity Relationships) program, was weaker than that without Cl^{-}. The prepared GR/β-CD composite revealed great advantages in photoelectrocatalytic degradation of organic pollutants due to its metal-free, low cost, simplicity, and efficient performance. This work provided new insight into the efficient and safe degradation of organic pollutants in wastewaters.

1. Introduction

Organic dye pollutants from industrial effluents in the textile, paper, plastic, and many other industries, have attracted much attention due to their threats to the environment as well as living organisms even at low concentrations.[1] The treatment methods and technologies of water or wastewater contaminated by organic dyes have been researched in previous studies, such as the advanced oxidation processes (AOPs), including ozonation, Fenton and UV/H$_2$O$_2$ treatments. Photocatalysis, and photoelectrocatalysis, are efficient removal technologies for wastewater containing organic dyes and many other organic pollutants.[2–6] Among these AOPs, photoelectrocatalytic technology has proven to be an efficient method to degrade organic

contaminants,[7,8] and it achieves photocatalysis by applying a biased voltage on the catalysts.[9]

Graphene (GR)-based semiconductor composites have been confirmed to be efficient catalysts in the photoelectrocatalytic process from a vast number of applications for pollutant degradation.[10–12] Semiconductor, *e.g.* Titania (TiO$_2$), in the composites could induce the generation of electrons and holes under light irradiation.[13,14] The fast recombination of the electron/hole pairs could be avoided in the photoelectrocatalysis process by applying an external bias potential.[15] In addition, GR could potentially increase the separation efficiency of the electron/hole pairs, due to the high conductivity and superior electron mobility.[16,17] Thus, the generated electrons in the valence band of the semiconductor were easily transferred to the conduction band of GR in the photoelectrocatalytic process with the GR-based nanocomposites as catalysts.[18,19] The generation of hydroxyl radical ($^{\bullet}$OH), superoxide radical (O$_2^{\bullet-}$), and hydrogen peroxide (H$_2$O$_2$) were induced by the positive holes in the semiconductor and the negative electrons in the GR, and organic pollutants could be degraded into less reactive molecules by them.[11]

Graphene oxide (GO) and reduced graphene oxide (RGO) nanostructures were also the photocatalytically active materials.[20,21] The fully oxidized GR was an insulator, while partially

[a]School of Municipal and Environmental Engineering, Jilin Jianzhu University, Research Field: Environmental Chemistry, Changchun 130118, China. E-mail: congqiao@jlju.edu.cn

[b]School of Environment, Northeast Normal University, Research Field: Environmental Chemistry, No. 2555 Jingyue Street, Changchun 130117, China. E-mail: renm677@ nenu.edu.cn; zhangtt671@nenu.edu.cn; Chengfy310@nenu.edu.cn; quj100@nenu. edu.cn; Fax: +86 431 89165610; Tel: +86 431 89165617

† Electronic supplementary information (ESI) available. See DOI: 10.1039/d1ra04533d

oxidized graphene was a semiconductor.[22] The GO, with a bandgap of 3.26 eV, was synthesized and used to induce the photocatalytic reduction of Resorufin to Resorufin.[20] GO and RGO have been proved to be the convenient metal-free carbon catalyst.[23–25] Nitrogen-doping on the GR could further enhance its photocatalytic activity.[26] In our previous study, GR was prepared by solvothermal method and using grass (*Festucaar- undinace*) as the sole carbon resource.[27] The prepared GR was found to be copper- and nitrogen-doped on its surface, which could be used to remove 2-chlorophenol by the oxidation of the generated $O_2{}^{\cdot-}$ and $\cdot OH$. Thus, the prepared GR was an efficient photocatalyst. The above findings prompted our interest to study the photoelectrocatalytic performance of the prepared GR and to enhance the efficiency of the photocatalyst.

However, the GR was tended to form irreversible agglomerates and even restack through van der Waals interactions, due to its high hydrophobic property.[28] Therefore, designing and introducing a new functional molecule for effective dispersing GR and loading the GR or GR-based photoelectrocatalyst on the electrode is highly desirable and technologically important. The beta-cyclodextrin (β-CD) was well known for selectively combining with various organic and inorganic guest molecules, due to its toroidal morphology, the hydrophobic inner cavity, and hydrophilic exterior.[29,30] Meanwhile, β-CD had been considered to be nontoxic, biodegradable, and without secondary environmental concerns.[31] Thus, β-CD was widely applied to design electrochemical sensors, adsorbents, and catalysts.[32,33] The composite of GR or GR-based semiconductor and β-CD was frequently used as electrochemical sensors[34] and was expected to apply in the field of electrocatalysis.[29]

With bromophenol blue (BPB) as the model pollutant (details were shown in Text S1 in ESI†), GR/β-CD composite was prepared and used as a catalyst to degrade BPB in water. BPB was a triphenylmethane derivative that was usually used as industrial dyes for foods, drugs, cosmetics, textiles, printing inks, and laboratory indicators,[35] but whose degradation pathways were seldom reported. In this work, the prepared GR/β-CD composite material could effectively degrade BPB in water in a photoelectric catalytic system, and the catalytic efficiency was obviously influenced by the presence of Cl^- in water. The toxicities of identifying degradation intermediates and risk assessments of the photoelectrocatalytic processes were also predicted using the QSAR (Quantitative Structure–Activity Relationship) model of the Ecological Structure–Activity Relationships (ECOSAR) program. Thus, this work provides a scientific basis for the convenient degradation of organic pollutants in wastewater.

2. Materials and method

2.1 Materials and chemicals

β-CD and BPB were obtained from Tianjin Guangfu Fine Chemical Research Institute. Sodium dodecyl sulfate (SDS) was purchased from Tianjin Fuchen Chemical Reagents Factory. In addition, ethanol, nitric acid (HNO₃), hydrofluoric acid (HF), 4-benzoquinone (4-BQ), isopropanol, ethylenediaminetetraacetic acid disodium salt (EDTA-2Na), methanol, and NaCl were the

analytic purity and purchased from the Beijing Chemical Works. GR was prepared according to our previous reported literature,[27,36] and the preparation method was shown in Text S2 in ESI.† Only second distilled water was used in this study.

2.2 Preparation of GR/β-CD electrode

2.2.1 Synthesis of GR/β-CD composite. 2 mg SDS was added into deionized water (10 mL) with different doping amounts of GR (10, 20, and 30 mg) after being dispersed in the ultrasonic bath for 10 min. SDS was used to disperse uniformly the stable GR. Subsequently, β-CD (200 mg) was dropped into the above mixture and treated with ultrasound (100 kHz) at 25 °C for 1 h in a KQ5200E-type ultrasonic cleaner.

2.2.2 Preparation of GR/β-CD modified titanium mesh electrode. The surface of the titanium mesh (3 cm × 3 cm) was polished using the abrasive paper and ultra-sonicated (100 kHz) in second distilled water. Afterward, the titanium sheet was immersed in the mixture (the volume ratio was 1 : 4 : 5) of HF, HNO₃, and second distilled water. The treated titanium mesh was ultra-sonicated again in ethanol solution (99.7%) and dried in the air after being washed with second distilled water. Finally, the GR/β-CD composite (membrane on the titanium mesh) electrode was obtained by covering an appropriate amount (about 2 mg) of GR/β-CD suspension on the surface of the titanium mesh and dried in air.

2.3 Characterization

The GR/β-CD composite was characterized as follows: transmission electron microscopy (TEM, Tecnai G2 F20 S-TWIN, FEI) images were used to characterize the morphology and microstructure of GR/β-CD; UV-vis pattern was achieved using a UV-vis spectrophotometer (Cary 500 scan spectrophotometers, Varian); X-ray diffraction (XRD) patterns were obtained on a Rigaku D-max C III (monochromatic Cu radiation); Fourier transform infrared (FT-IR) spectra (4000–400 cm⁻¹) were performed using a Nexus 670 FT-IR spectrometer (Thermo Nicolet, Madison) equipped with a KBr beam splitter (KBr, FT-IR grade).

2.4 Photoelectrocatalytic degradation for BPB

The prepared GR/β-CD composite on the titanium mesh was put into 100 mL BPB (20 mg L⁻¹) solution in a quartz reactor and conducted on the EC550 electrochemical workstation (Wuhan Gaoss Union Technology Co., Ltd), which was connected to a three-electrode system using the Pt-column as the counter electrode, saturated calomel electrode as reference electrode, and the prepared GR/β-CD composite as working electrode. To ensure the adsorption–desorption equilibrium of BPB on the GR/β-CD composite, the BPB solution with the working electrode (no voltage) was stirred in the dark for 30 min.[37] Afterward, the quartz reactor was placed and irradiated with the simulated sunlight (Xenon lamp, 300 W), and the distance between them was 10 cm, and a condensate water circulation device was used to control the temperature at 25 ± 1 °C. The electrochemical workstation also provided relatively stable voltage in the process of the photoelectrocatalytic degradation for BPB. 3 mL samples were taken out at regular time intervals.

To test the performance for each pristine form of composite along with the final composite, the photoelectrocatalytic degradation experiment of β-CD was carried out. Due to its high hydrophobic property, GR cannot be used alone as a photoelectrocatalytic electrode. The removal rate (η) was calculated by the following equation:

$$\eta = (c_0 - c_t)/c_0 \times 100\%$$

where c_0 and c_t referred to the initial concentration and the concentration at time t, respectively. In some experiments, NaCl was added to investigate the Cl$^-$ effect on BPB photoelectrocatalytic degradation.

2.5 Mechanisms

To elucidate the mechanisms of photocatalytic and photoelectrocatalytic degradation for BPB by the prepared GR/β-CD composite on titanium mesh, 4-BQ (scavenger for O$_2$·$^-$, 1.0 mM),[38] isopropanol (scavenger for ·OH, 0.5 mM),[39] EDTA-2Na (scavenger for the hole, 0.5 mM),[40] and methanol (transforming agent for ·OH to ·HO$_2$/O$_2$·$^-$, 1.0 mM)[41] were added into BPB solutions, respectively.

2.6 Analytical methods

After a definite degradation time, the concentrations of BPB were determined at 590 nm (ref. 42) using single-wavelength detection of UV-visible spectrophotometer (UV-2450, Shimadzu Scientific Instruments, Japan), and the UV absorption spectrum of BPB was shown in Fig. S2 in ESI.† Furthermore, ultra-performance liquid chromatography-tandem mass spectrometry (UPLC-MS/MS, Waters Acquity UPLC/Quattro Premier XE), equipped with a Waters Acquity BET C$_{18}$ column (2.1 × 100 mm, 1.7 μm) at 45 °C, was applied to clearly identify the intermediates from catalytic degradation. The mobile phase was consisted of (A) 10 mM ammonium acetate and (B) acetonitrile, with the total flow rate at 0.25 mL min^{-1}. Gradient elution was

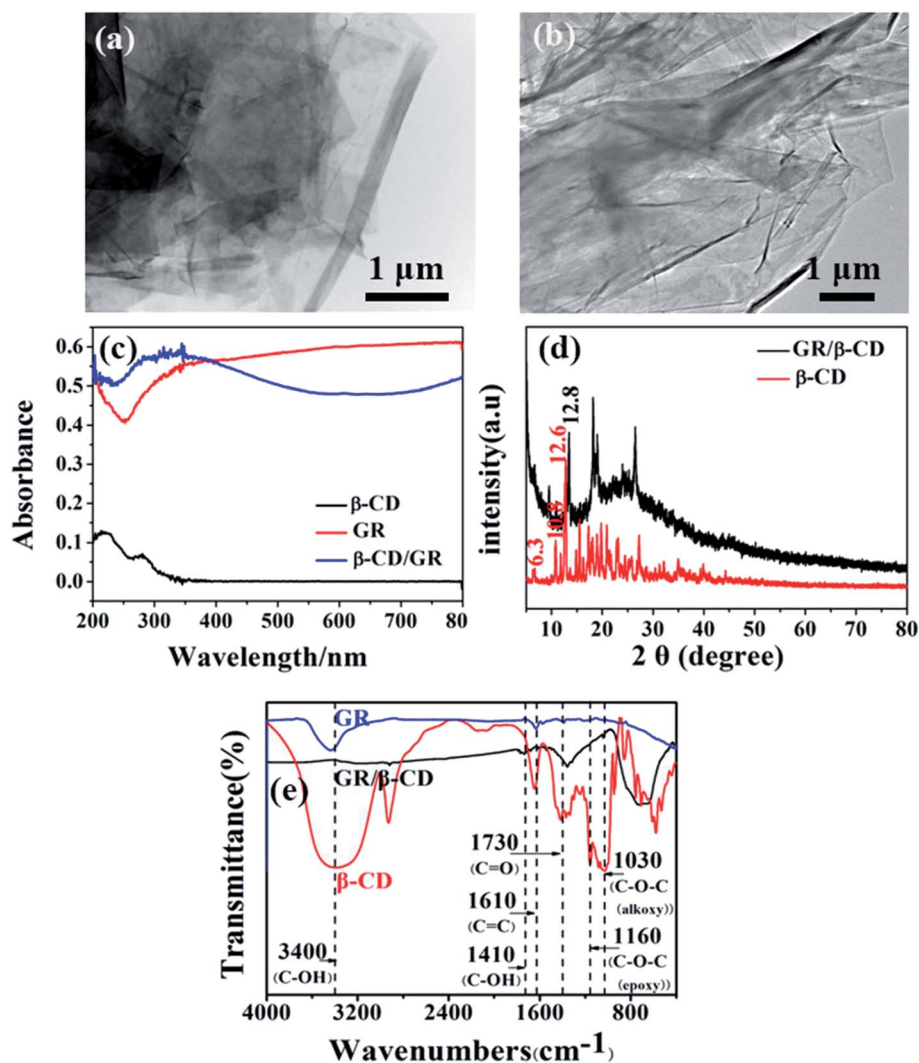Fig. 1 Characterization of the prepared GR and GR/β-CD composite: (a) TEM image of GR; (b) TEM image of GR/β-CD composite; (c) UV–Vis patterns of the GR, β-CD, and GR/β-CD composite; (d) XRD patterns of the β-CD and GR/β-CD composite; (e) FT–IR patterns of the GR, β-CD, and GR/β-CD composite.

set as follows: the initial concentration of solvent A was 97% and lasted for 4 min, then declined to 82% in 11 min, and in the subsequent 7 min, the concentration of solvent A declined to 60% and followed by a linear gradient to 20% A in 8 min. In the subsequent 1 min, the concentration of solvent A declined to 5%. After maintenance for 9 min, the solvent A was recovered to 97% within 0.1 min. The total elapsed time was 44 min.

2.7 Toxicity assessment

QSAR was used to assess the acute and chronic toxicities of intermediates from the catalytic degradation. The toxicities of intermediates were calculated to three trophic levels of aquatic organisms including fish, daphnia, and green algae using the ECOSAR program in combination with the EPIWIN (Estimation Programs Interface for Windows) software.[43] Particularly, acute and chronic toxicities were expressed using EC_{50} values (the pollutant concentration that inhibited green algae growth by 50% after 96 h) and LC_{50} values (the pollutant concentration that led to the death of 50% fish and daphnia after 96 and 48 h exposure, respectively). For conservative consideration, the lowest effective concentration was used in the toxicity assessment.

2.8 Statistical analysis

To determine the credibility of the experimental results, each experiment was repeated at least three times. The error bars display the 95% confidence interval for $n = 3$. The relative error bar displays the standard deviation from the mean. The Student's t-test (two-tailed) is applied to determine the significance of the difference between degradations. At the 95% confidence level, the difference is considered significant ($p < 0.05$).

3. Results and discussion

3.1 Characterization of prepared GR/β-CD composite

The TEM images of GR and GR/β-CD composite were shown in Fig. 1(a) and (b), respectively. The transparent and crumpled GR was prepared and dispersed on the surface of β-CD. The light absorption of β-CD was weak at $\lambda < 350$ nm, but the prepared GR/β-CD composite (10% GR) revealed a broad and strong light absorption from 250 to 400 nm, which could be attributed to the doped GR (as shown in Fig. 1(c)). The analysis results of XRD

were shown in Fig. 1(d), where the GR/β-CD has observed the characteristic peaks in the range of $2\theta = 5$–30° and 12.8°, which corresponding to the crystalline structure of β-CD and GR.[44] It can be seen that typical β-CD absorption peaks of the ring vibrations at 578 and 721 cm^{-1} from the FT-IR spectrum of GR/β-CD (Fig. 1(e)), the coupled C–O–C stretching and O–H bending vibration at 1172 cm^{-1}, and the CH_2 stretching vibration at 2920 cm^{-1},[45] respectively. C=C conjugation (1541 cm^{-1}) and the C–OH band (1398 cm^{-1}) in GR were also obviously observed,[46] and the vibration peak at 1735 cm^{-1} corresponds to the peak of C=O, which indicates that there is a conjugated bond in GR/β-CD. At the same time, the large conjugate bond also promotes electron transfer. In GR/β-CD, the positions of these peaks shifted to lower wavenumbers, indicating that the strength of C–OH, C=C, and C–O–C bands bonds are weaker.[10] β-CD contains hydroxyl groups, which easily form the hydrogen bond between the hydroxyl groups on β-CD and the ether bond on adjacent β-CD or GR. Therefore, the β-CD diffraction peaks of cyclodextrin for GR/β-CD inconsistent with blank β-CD. New diffraction peaks appeared in XRD, confirmed that the GR/β-CD composite was prepared successfully.

3.2 Photoelectrocatalytic degradation for BPB and influence factors

BPB (20 mg L^{-1}) was removed efficiently by the prepared GR/β-CD composite (shown in Fig. 2). The effect of β-CD amount on the photoelectrocatalytic degradation efficiency for BPB was obvious. The photoelectrocatalytic degradation efficiencies (Fig. 2(a)) of the β-CD/GR composite for BPB were $82.4 \pm 1.7\%$, $89.5 \pm 3.3\%$, and $73.4 \pm 3.5\%$ with the β-CD dosage of 100, 200, and 400 mg, respectively, within 180 min. The low loading level of β-CD deviated from stoichiometry with inclusion complexes formed by GR. In addition, the high loading level of β-CD could not keep the high conductivity and reduce the effective active sites of the catalyst relatively. The photoelectrocatalytic degradation efficiency was 22.8% only by β-CD within 180 min. However, the efficiencies (Fig. 2(b)) of the GR/β-CD for BPB were $67.3 \pm 2.6\%$, $89.5 \pm 3.3\%$, and $81.9 \pm 7.8\%$ with GR doping amount of 5%, 10%, and 15%, respectively, within 180 min. With the increasing dosage of GR, the degradation efficiency was increased, due to emerging more active sites of the catalyst. However, the degradation efficiency was decreased when the GR
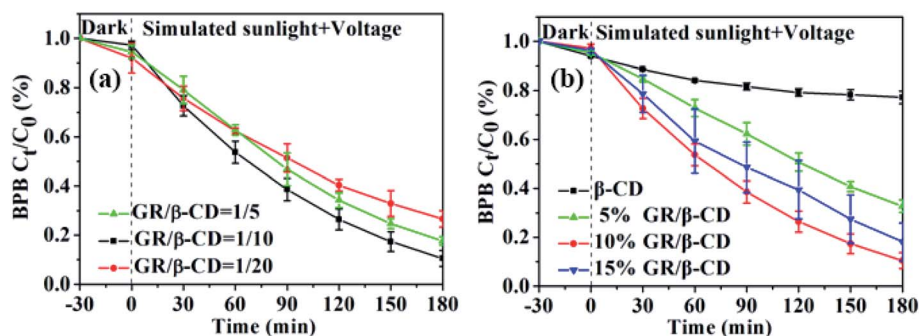

Fig. 2 Effects of different dosages of GR (a) and β-CD (b) on photoelectrocatalytic degradation kinetics for BPB.
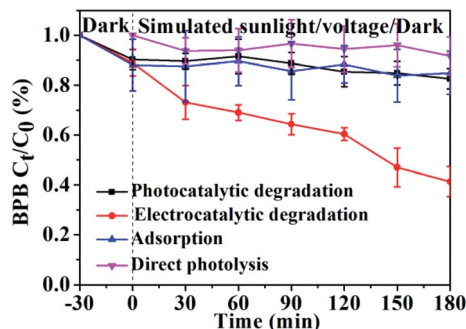
Fig. 3 Adsorption, photolysis, photocatalytic, electrocatalytic, and photoelectrocatalytic degradation for BPB.

dosage was above 10%, which was attributed to overlapping or aggregation of active sites resulting in a decrease in total degradation area available to BPB molecule. In addition, the degradation efficiency was increased with the increasing dosage of GR, due to emerging more active sites of the catalyst. As the results, dosages of 200 mg β-CD and 10% GR were the most suitable amount to use in the following studies, unless otherwise specified.

The performances of photocatalytic, electrocatalytic, and photoelectrocatalytic degradation for BPB (20 mg L^{-1}) by the prepared GR/β-CD composite were shown in Fig. 3. Within 180 min, the photocatalytic degradation efficiency was only 16.5 ± 4.1%, and the electrocatalytic degradation efficiency was 59.5 ± 6.0%. The results indicated that the degradation efficiencies of photocatalytic and electrocatalytic BPB were lower than photoelectrocatalytic (Fig. 2). The reported photocatalytic

degradation efficiency of BPB was 94.5% within 10 h by chitosan conjugated magnetic nanoparticles[47] and 32.0% within 3 h by CuO-nano-clinoptilolite composite.[48] Therefore, the photoelectrocatalytic degradation efficiency for BPB by the prepared β-CD/GR composite was successful and efficient.

The influences of voltage, initial concentration, and pH (adjusted by HNO$_3$) on the photoelectrocatalytic degradation efficiency of BPB by the GR/β-CD composite were shown in Fig. 4. The photoelectrocatalytic degradation efficiencies of the GR/β-CD composite for BPB (20 mg L^{-1}) within 180 min were 60.0 ± 6.1%, 89.5 ± 3.3%, 85.9 ± 1.0%, 89.6 ± 0.3%, and 94.0 ± 1.8% with an initial voltage of 2, 4, 6, 8, and 10 V, respectively. The direct photolysis efficiency was 8.3% (shown in Fig. 3) with simulated sunlight irradiation for 180 min. The results further confirmed the important role of external biasing voltage, which promoted the separation of photoelectrons from vacancies.[15] Meanwhile, the enriched electrons on GR in the composite could react with H$_2$O and dissolved O$_2$, leading to the generation of reactive oxygen species (ROS).[11] So, 4 V biasing voltage was used in the following work.

The photoelectrocatalytic degradation efficiency for BPB was decreased with the increasing concentrations (Fig. 4(b)). The negative effect of initial concentration on the degradation of dyes was also reported in the previous researches,[49] owing to the following two reasons: first, with the increasing of the initial concentration of BPB, more BPB molecules were adsorbed onto the surface of GR/β-CD composite, but the adsorbed BPB molecules could not be degraded immediately, which led to the decreasing of the active sites;[50] secondly, the solution became more intensely colored, and thereby fewer photons reached the catalyst surface.[51] Therefore, the photo-induced degradation
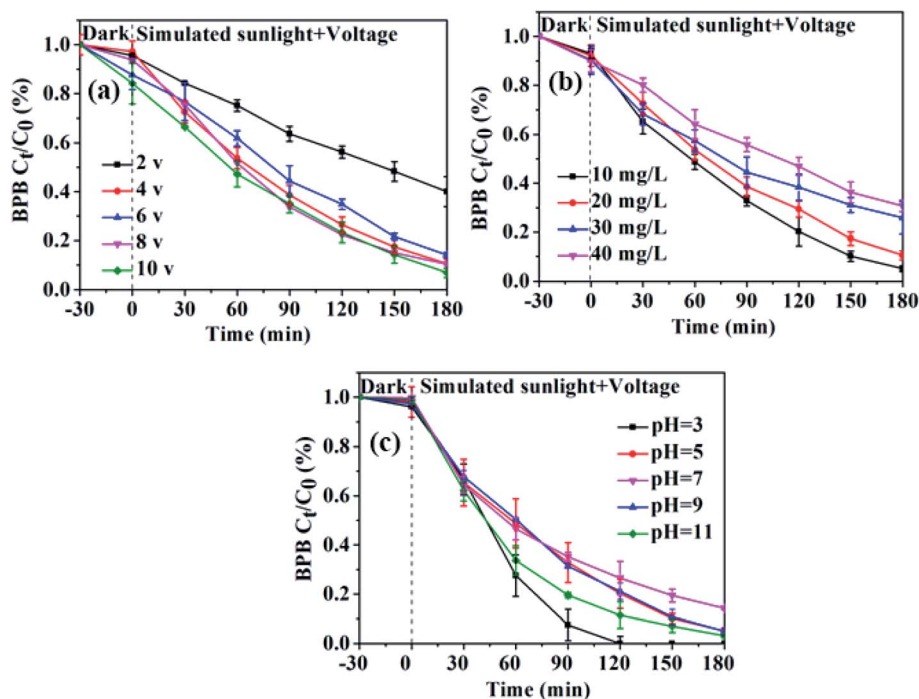

Fig. 4 Effect of voltage (a), initial concentration (b); and pH (c) on photoelectrocatalytic degradation of the GR/β-CD for BPB.
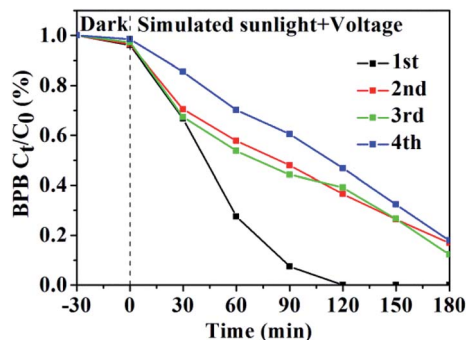
Fig. 5 Stability of the prepared GR/β-CD for BPB photoelectrocatalytic degradation.

efficiency was reduced with the increasing concentration. As a result, 10 mg L^{-1} BPB was opportunely used in the following studies.

As shown in Fig. 4(c), the BPB (10 mg L^{-1}) degradation efficiency was decreased as the pH increase from 3.0 to 7.0, and then increased with the pH increasing from 7.0 to 11.0. The degradation efficiency of BPB could reach almost 100% within 120 min at pH 3.0. The dissociation forms of the BPB were different at the different pH values.[52] Thus, the difference in degradation efficiency for BPB in different pH solutions was supposed to be attributed to its dissociation. The pH of the BPB solution played a dominant role in the photoelectrocatalytic degradation of BPB, compared with voltage and initial concentration. Hence, pH 3.0 was optimally selected in the following experiment.

The stability of the catalyst was an important factor to evaluate the effect of photoelectrocatalysis. The catalytic efficiency of the prepared GR/β-CD composite for BPB was 51.5% with simulated sunlight irradiation for 120 min and was also maintained to be above 82.0% at 180 min (Fig. 5) after being recycled three times. Due to the processes of photoelectrocatalytic degradation happened, the film is gradually broken off and the photoelectrocatalytic degradation property decreases.

3.3 Mechanism of photoelectrocatalytic degradation for BPB

Quenching experiments were performed to elucidate the important roles of ROS generated by the GR/β-CD composite in

the photoelectrocatalytic system. The photoelectrocatalytic degradation efficiencies for BPB in pH 3.0 solutions within 120 min decreased from 100% to 58.5 ± 3.9%, 9.3 ± 1.1%, 27.5 ± 5.7%, and 25.8 ± 5.6% with the presence of 4-BQ, isopropanol, methanol, and EDTA-2Na, respectively (Fig. 6(a)), meant that the roles of ROS for photoelectrocatalytic degradation of BPB at pH 3.0 were ruled according to the following sequence: $O_2^{\cdot-}$ > h^+ > $^{\cdot}HO_2$ > $^{\cdot}OH$. At pH 7.0, the photoelectrocatalytic degradation efficiencies for BPB within 180 min decreased to 60.9 ± 6.1%, 16.8 ± 6.3%, 18.5 ± 5.5%, and 48.8 ± 10.8% with 4-BQ, isopropanol, methanol, and EDTA-2Na, respectively (Fig. 6(b)), indicated that $O_2^{\cdot-}$ also played the important role in the photoelectrocatalytic degradation for BPB at pH 7.0.

With the combination of the simulated sunlight irradiation and GR, the generated excited electrons could react with H_2O and O_2 to produce $^{\cdot}OH$ and $O_2^{\cdot-}$. In addition, the generated h^+ also reacted with H_2O to produce $^{\cdot}OH$ at the same time. With the presence of external voltage and simulated sunlight irradiation, the accumulated photo-induced e^- on GR could be trapped by O_2 molecules and lead to the generation of $O_2^{\cdot-}$. $O_2^{\cdot-}$ was the most important precursor of $^{\cdot}OH$ and $O_2^{\cdot-}$ therefore, $O_2^{\cdot-}$ played the most important role in the photoelectrocatalytic degradation of the prepared GR/β-CD composite for BPB.

As shown in previous studies, Cl$^-$ could influence the generation of reactive species.[53] Chlorine radicals ($^{\cdot}Cl$ and $^{\cdot}Cl_2^-$), formed from the Cl$^-$ in water by oxidation of $^{\cdot}OH$,[54] could induce the degradation of organic pollutants and form chlorinated intermediates.[12,55] Therefore, the influence of the specific chloride ion effect on the degradation of BPB (10 mg L^{-1}) by the prepared GR/β-CD composite was investigated by adding NaCl (0.05, 0.2 mol L^{-1}). As shown in Fig. 7, the presence of Cl$^-$ slightly promoted the BPB degradation at pH 3.0 and 7.0. The photoelectrocatalytic degradation efficiencies for BPB within 180 min at pH 7.0 were increased from 85.8% to 94.9% with 0.05 mol L^{-1} Cl$^-$, and to 92.2% with 0.2 mol L^{-1} Cl$^-$, respectively. As a result, the time needed for removing all BPB at pH 3.0 was decreased from 90 min to 60 min with 0.05 mol L^{-1} Cl$^-$, and to 30 min with 0.2 mol L^{-1} Cl$^-$, respectively. The results meant that Cl$^-$ in waste could promote the photoelectrocatalytic degradation of the prepared GR/β-CD composite
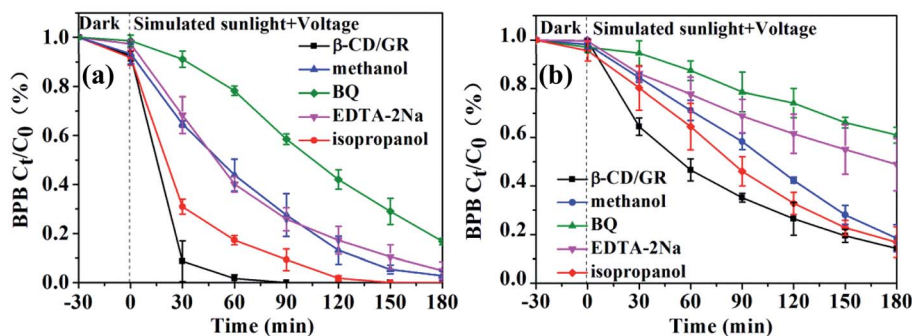

Fig. 6 Plotted photoelectrocatalytic degradation curves of the GR/β-CD composite for BPB with scavengers: (a) pH = 3.0; (b) pH = 7.0.
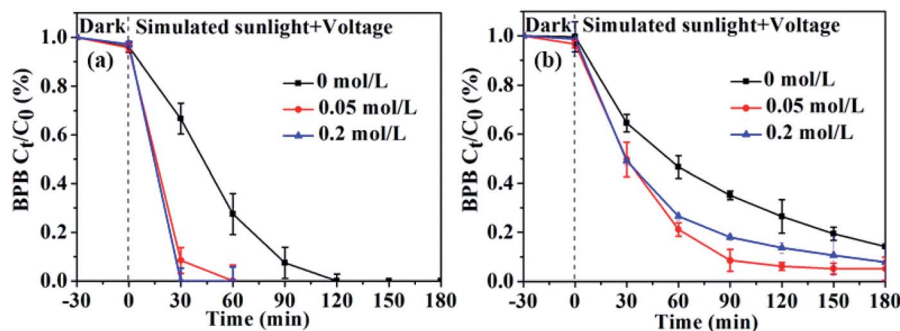
Fig. 7 Plotted photoelectrocatalytic degradation curves of the GR/β-CD composite for BPB with Cl^- at: (a) pH 3.0; (b) pH = 7.0.

for BPB, especially at low pH. But the promotion effect is very little, the experimental result reported is in agreement with literature results.[56]

As shown above, $^{\cdot}OH$ played a minor role in BPB degradation by the prepared GR/β-CD composite in the photoelectrocatalysis processes. While $^{\cdot}OH$ could oxidize Cl^- and form $^{\cdot}Cl$ and $^{\cdot}Cl_2^-$ through a series of chain reactions.[54] The generated chlorine radicals could undergo a fast reaction with aromatic compounds (second-order reaction rate constants of 10^7 to 10^{10} M^{-1} s^{-1}).[57] The chloride ion concentration in this work is 0.05 M, which is much higher than that of BPB. $^{\cdot}Cl$ and $^{\cdot}Cl_2^-$ are less reactive and more selective than $^{\cdot}OH$. They can effectively attack electron-rich compounds or groups. The BPB molecule has three benzene rings connected by C–O, two of which are substituted by bromine atoms, and the other is a benzene ring

with the O=S=O group. The benzene ring with two bromine atom substituents lacks electrons, which is not conducive to the attack of $^{\cdot}Cl$ and $^{\cdot}Cl_2^-$. In the case of another benzene ring, the O=S=O group is electron withdrawing, although C–O donates electrons, the electron-withdrawing ability of dibromide is strong, so C–O may not be able to provide electrons to the benzene ring together with O=S=O. Therefore, the benzene ring with O=S=O group is not easy to be corroded by $^{\cdot}Cl$ and $^{\cdot}Cl_2^-$.[58] Therefore, Cl^- in water marginally increased the photoelectrocatalytic degradation efficiency for BPB. The dismutation reaction of $O_2^{\cdot-}$ to form $^{\cdot}OH$ was preferred to proceed in solutions with high H^+ concentrations.[59] Thus, the effect of Cl^- in water on the acceleration of BPB degradation under acid conditions was more significant than neutral.

Table 1   Identified intermediates of photoelectrocatalytic degradation for BPB

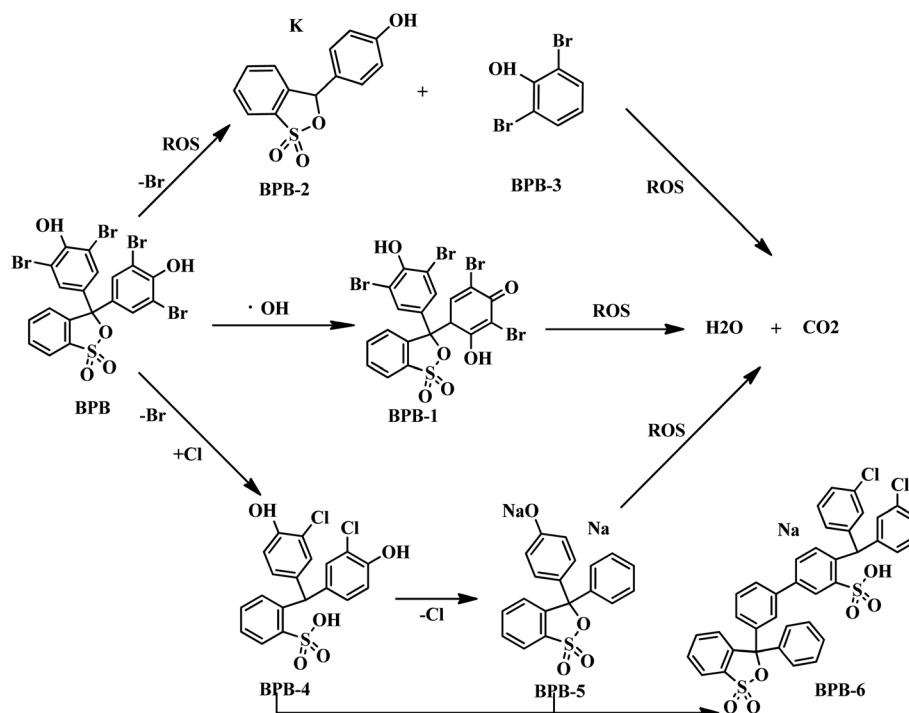| Product without Cl^-	Molecular weight	Structure	Product with Cl^-	Molecular weight	Structure
BPB-1	685.97		BPB-4	425.28	
BPB-2	301.38				
BPB-3	251.90		BPB-6	736.64	
BPB-5	361.37				

Fig. 8 Possible degradation pathways of BPB catalyzed by the GR/β-CD composite.

Table 2 Results of toxicity assessments for the degradation intermediates[a]

Products	Acute toxicity (mg L⁻¹)			Chronic toxicity (ChV) (mg L⁻¹)		
	Fish (LC$_{50}$)	Daphnid (LC$_{50}$)	Green algae (EC$_{50}$)	Fish	Daphnid	Green algae
BPB	0.172	0.019	0.049	0.005	0.035	0.058
BPB-1	4.954	7.639	2.561	0.260	2.715	1.334
BPB-2	34.888	71.554	30.442	3.121	44.957	7.714
BPB-3	4.247	2.438	9.891	0.468	0.463	4.571
BPB-4	194.142	680.002	32.421	55.292	249.817	8.494
BPB-5	182.598	426.936	202.589	20.860	348.414	36.896
BPB-6	0.757	0.772	0.183	0.018	0.120	0.271

[a] The predicted toxicity values are classified according to the system established by the globally harmonized system of classification and labeling of chemicals (GHS): white boxes, not harmful: $LC_{50}/EC_{50}/ChV > 100$; light grey boxes, harmful: $100 \geq LC_{50}/EC_{50}/ChV > 10$; medium grey boxes, toxic: $10 \geq LC_{50}/EC_{50}/ChV > 1$; dark grey boxes, very toxic: $LC_{50}/EC_{50}/ChV \leq 1$.[60]

3.4 Degradation intermediates and toxicity assessment

The photoelectrocatalytic degradation intermediates of BPB were identified with UPLC-MS/MS (Fig. S3 in ESI†), and the main degradation intermediates are shown in Table 1.

Based on the determination of intermediates, the proposed degradation pathways of BPB are shown in Fig. 8. The main photoelectrocatalytic degradation pathways of BPB were debromination and C–C bond cleavage. Based on the determination of intermediates, the proposed degradation pathways of BPB are shown in Fig. 8. BPB can undergo photoelectrocatalytic degradation mainly through the pathways as shown below: the first one is hydrolysis which leads to the generation of BPB-1. The second one is C–C bond cleavage which leads to the generation of BPB-4 and BPB-5 (2,6-dibromophenol). The third one is chlorination which leads to the generation of BPB-2 in the presence of Cl⁻. Besides, BPB can undergo debromination as the identified products with lower Br numbers compared with BPB. The formed BPB-2 can undergo a dechlorination reaction leading to the generation of BPB-3. Furthermore, a polymerization product BPB-6 was generated *via* coupling reactions from BPB-2 and BPB-3. In a conclusion, the main photoelectrocatalytic degradation pathways of BPB were hydrolysis, debromination, C–C bond cleavage, and chlorination. The identification of chlorine-containing intermediates further confirmed the involvement of chlorine radicals in the photoelectrocatalytic degradation of BPB in the presence of Cl⁻.

Toxicities of BPB and intermediates were calculated based on QSAR using ECOSAR program, due to the lack of commercial standards of most intermediates. As illustrated in Table 2, the predicted toxicities of all the identified intermediates were lower than BPB. Among the degradation intermediates, the toxicity of BPB-6 was the strongest, whereas the calculated LC_{50}/EC_{50}/ChV (chronic toxicity) value of BPB-6 was approximately ten to hundred times lower than BPB in water for fish, daphnid, and green algae. The results of toxicity assessment indicated that the potential risks to the aquatic organism and human health of BPB were reduced in the photoelectrocatalytic processes by the prepared GR/β-CD composite.

4. Conclusions

The prepared GR/β-CD composite was proved to be an efficient catalyst for BPB degradation in photoelectroncatalytic process. The best doping amount of GR in GR/β-CD composite was 10%, and the photoelectrocatalytic degradation efficiency of BPB reached 100% at pH 3 within 120 min, with the combination of the applied voltage of 4 V and simulated sunlight irradiation. In addition, the time needed for removal of all BPB in water could be decreased to 60 min, and even 30 min with Cl⁻ in water. The $\cdot O_2^-$ played the dominant role in photoelectrocatalytic degradation of the prepared GR/β-CD composite for BPB. Degradation intermediates were identified from the photoelectrocatalytic degradation for BPB, and their toxicities were predicted to be reduced compared with BPB. Therefore, the prepared GR/β-CD composite revealed great advantages in photoelectrocatalytic degradation of organic pollutants due to

its metal-free, low cost, easily synthesized, convenient, simplicity, efficient performance, and broad applicability, which could be widely applied in the treatment of refractory organics in the wastewater.

Conflicts of interest

There are no conflicts to declare.

Acknowledgements

References

1 J. Wang and R. Bai, *Water Res.*, 2016, **101**, 103–113.
2 E. Brillas and C. A. Martínez-Huitle, *Appl. Catal., B*, 2015, **166–167**, 603–643.
3 J. C. Cardoso, G. G. Bessegato and M. V. Boldrin Zanoni, *Water Res.*, 2016, **98**, 39–46.
4 W. H. Glaze, J.-W. Kang and D. H. Chapin, *Ozone: Sci. Eng.*, 1987, **9**, 335–352.
5 X. Guo, D. Minakata, J. Niu and J. Crittenden, *Environ. Sci. Technol.*, 2014, **48**, 5718–5725.
6 M. M. Huber, S. Canonica, G.-Y. Park and U. von Gunten, *Environ. Sci. Technol.*, 2003, **37**, 1016–1024.
7 S. Garcia-Segura and E. Brillas, *J. Photochem. Photobiol., C*, 2017, **31**, 1–35.
8 X. Meng, Z. Zhang and X. Li, *J. Photochem. Photobiol., C*, 2015, **24**, 83–101.
9 P. Wang, Y. Ao, C. Wang, J. Hou and J. Qian, *J. Hazard. Mater.*, 2012, **223–224**, 79–83.
10 W. Cui, J. He, H. Wang, J. Hu, L. Liu and Y. Liang, *Appl. Catal., B*, 2018, **232**, 232–245.
11 V. Kumar, K.-H. Kim, J.-W. Park, J. Hong and S. Kumar, *Chem. Eng. J.*, 2017, **315**, 210–232.
12 Y. Zhang, W. Cui, W. An, L. Liu, Y. Liang and Y. Zhu, *Appl. Catal., B*, 2018, **221**, 36–46.
13 K. Zhu, N. Neale, a. Miedaner and A. Frank, *Nano Lett.*, 2007, **7**, 69–74.
14 H.-F. Zhuang, C.-J. Lin, Y.-K. Lai, L. Sun and J. Li, *Environ. Sci. Technol.*, 2007, **41**, 4735–4740.
15 S. Yu, M. Xi, K. Han, Z. Wang, W. Yang and H. Zhu, *Thin Solid Films*, 2010, **519**, 357–361.
16 E. Kecsenovity, B. Endrődi, P. S. Tóth, Y. Zou, R. A. W. Dryfe, K. Rajeshwar and C. Janáky, *J. Am. Chem. Soc.*, 2017, **139**, 6682–6692.
17 Q. Xiang, J. Yu and M. Jaroniec, *Chem. Soc. Rev.*, 2012, **41**, 782–796.
18 A. Adán-Más and D. Wei, *Nanomaterials*, 2013, **3**, 325–356.

19 R. Atchudan, T. N. Jebakumar Immanuel Edison, S. Perumal, D. Karthikeyan and Y. R. Lee, *J. Photochem. Photobiol., A*, 2017, **333**, 92–104.

20 K. Krishnamoorthy, R. Mohan and S. J. Kim, *Appl. Phys. Lett.*, 2011, **98**, 3.

21 H. Sun, S. Liu, G. Zhou, H. M. Ang, M. O. Tadé and S. Wang, *ACS Appl. Mater. Interfaces*, 2012, **4**, 5466–5471.

22 K. P. Loh, Q. Bao, G. Eda and M. Chhowalla, *Nat. Chem.*, 2010, **2**, 1015–1024.

23 D. R. Dreyer, H. P. Jia and C. W. Bielawski, *Angew. Chem. Int. Ed.*, 2010, **49**, 6813–6816.

24 G. Lv, H. Wang, Y. Yang, T. Deng, C. Chen, Y. Zhu and X. Hou, *ACS Catal.*, 2015, **5**, 5636–5646.

25 C. Su, M. Acik, K. Takai, J. Lu, S. J. Hao, Y. Zheng, P. Wu, Q. Bao, T. Enoki, Y. J. Chabal and K. P. Loh, *Nat. Commun.*, 2012, **3**, 1298.

26 X. G. Duan, Z. M. Ao, H. Q. Sun, S. Indrawirawan, Y. X. Wang, J. Kang, F. L. Liang, Z. H. Zhu and S. B. Wang, *ACS Appl. Mater. Interfaces*, 2015, **7**, 4169–4178.

27 Y. Ma, N. Lu, Y. Lu, J. N. Guan, J. Qu, H. Y. Liu, Q. Cong and X. Yuan, *Sci. Rep.*, 2016, **6**, 14.

28 J. Yan, J. Liu, Z. Fan, T. Wei and L. Zhang, *Carbon*, 2012, **50**, 2179–2188.

29 Z. Liu, Q. Xue and Y. Guo, *Biosens. Bioelectron.*, 2017, **89**, 444–452.

30 M. V. Rekharsky and Y. Inoue, *Chem. Rev.*, 1998, **98**, 1875–1918.

31 H. Liu, X. Cai and J. Chen, *Environ. Sci. Technol.*, 2013, **47**, 5835–5842.

32 X. Cai, Q. Liu, C. Xia, D. Shan, J. Du and J. Chen, *Environ. Sci. Technol.*, 2015, **49**, 9264–9272.

33 Z. Zhang, S. Gu, Y. Ding, M. Shen and L. Jiang, *Biosens. Bioelectron.*, 2014, **57**, 239–244.

34 Y. Guo, S. Guo, J. Ren, Y. Zhai, S. Dong and E. Wang, *ACS Nano*, 2010, **4**, 4001–4010.

35 I. A. Salem, *Appl. Catal. B Environ.*, 2000, **28**, 153–162.

36 J. Qu, C. Luo, Q. Cong and X. Yuan, *Environ. Chem. Lett.*, 2012, **10**, 153–158.

37 N. Lu, Y. Zhao, H. Liu, Y. Guo, X. Yuan, H. Xu, H. Peng and H. Qin, *J. Hazard. Mater.*, 2012, **199–200**, 1–8.

38 A. C. Herath, R. M. G. Rajapakse, A. Wicramasinghe and V. Karunaratne, *Environ. Sci. Technol.*, 2009, **43**, 176–180.

39 R. I. Samoilova, A. R. Crofts and S. A. Dikanov, *J. Phys. Chem. A*, 2011, **115**, 11589–11593.

40 Y. Yu, D. Zhou and F. Wu, *Chem. Eng. J.*, 2015, **281**, 892–899.

41 C. Pan and Y. Zhu, *Environ. Sci. Technol.*, 2010, **44**, 5570–5574.

42 H. Khan, A. K. Khalil, A. Khan, K. Saeed and N. Ali, *Korean J. Chem. Eng.*, 2016, **33**, 2802–2807.

43 Q. Sui, W. Gebhardt, H. F. Schröder, W. Zhao, S. Lu and G. Yu, *Environ. Sci. Technol.*, 2017, **51**, 2262–2270.

44 N. Meng, Y. Su, N. Zhou, M. Zhang, M. Shao, Y. Fan, H. Zhu, P. Yuan, C. Chi and Y. Xiao, *Int. J. Biol. Macromol.*, 2016, **93**, 117–122.

45 E. Zor, M. Esad Saglam, S. Alpaydin and H. Bingol, *Anal. Methods*, 2014, **6**, 6522–6530.

46 L. Jiang, Y. Liu, S. Liu, X. Hu, G. Zeng, X. Hu, S. Liu, S. Liu, B. Huang and M. Li, *Chem. Eng. J.*, 2017, **308**, 597–605.

47 H. Khan, A. K. Khalil, A. Khan, K. Saeed and N. Ali, *Korean J. Chem. Eng.*, 2016, **33**, 2802–2807.

48 A. Nezamzadeh-Ejhieh and H. Zabihi-Mobarakeh, *J. Ind. Eng. Chem.*, 2014, **20**, 1421–1431.

49 L. B. Reutergådh and M. Iangphasuk, *Chemosphere*, 1997, **35**, 585–596.

50 B. Neppolian, H. C. Choi, S. Sakthivel, B. Arabindoo and V. Murugesan, *J. Hazard. Mater.*, 2002, **89**, 303–317.

51 O. K. Mahadwad, P. A. Parikh, R. V. Jasra and C. Patil, *Bull. Mater. Sci.*, 2011, **34**, 551–556.

52 A. Z. Dangui, V. M. S. Santos, B. S. Gomes, T. S. de Castilho, K. P. Nicolini and J. Nicolini, *Spectrochim. Acta Mol. Biomol. Spectrosc.*, 2018, **203**, 333–341.

53 Y. Li, J. Zhao, E. Shang, X. Xia, J. Niu and J. Crittenden, *Environ. Sci. Technol.*, 2018, **52**, 4842–4849.

54 K. M. Parker and W. A. Mitch, *Proc. Natl. Acad. Sci. U. S. A.*, 2016, **113**, 5868–5873.

55 Y. Li, X. Qiao, Y.-n. Zhang, C. Zhou, H. Xie and J. Chen, *Water Res.*, 2016, **102**, 405–412.

56 L. Gao, B. Zhou, F. Wang, R. Yuan, H. Chen and X. Han, *Environ. Sci. Pollut. Res.*, 2020, **27**, 2044–2053.

57 P. Neta, R. E. Huie and A. B. Ross, *J. Phys. Chem. Ref. Data*, 1988, **17**, 1027–1284.

58 Y. Rao, F. Han, Q. Chen, D. Wang, D. Xue, H. Wang and S. Pu, *Chemosphere*, 2019, **218**, 299–307.

59 D. Vione, M. Minella, V. Maurino and C. Minero, *Chemistry*, 2014, **20**, 10590–10606.

60 U. Nations, *Globally Harmonized System of Classification and Labelling of Chemicals (GHS)*, United Nations Publications, New York, 4th edn, 2011.